Comparative Thermodynamic Studies of Aqueous Glutaric Acid, Ammonium Sulfate and Sodium Chloride Aerosol at High Humidity[⊥]

Kate L. Hanford,[†] Laura Mitchem,[†] Jonathan P. Reid,*[,†] Simon L. Clegg,[‡] David O. Topping,[§] and Gordon B. McFiggans[§]

School of Chemistry, University of Bristol, Bristol, BS8 1TS, U.K., School of Environmental Sciences, University of East Anglia, Norwich NR4 7TJ, U.K., and School of Earth, Atmospheric and Environmental Sciences, University of Manchester, Williamson Building, Oxford Road, Manchester, M13 9PL, U.K.

Received: March 23, 2008; Revised Manuscript Received: May 14, 2008

Aerosol optical tweezers are used to simultaneously characterize and compare the hygroscopic properties of two aerosol droplets, one containing inorganic and organic solutes and the second, referred to as the control droplet, containing a single inorganic salt. The inorganic solute is either sodium chloride or ammonium sulfate and the organic component is glutaric acid. The time variation in the size of each droplet (3−7 μm in radius) is recorded with 1 s time resolution and with nanometre accuracy. The size of the control droplet is used to estimate the relative humidity with an accuracy of better than ±0.09%. Thus, the Köhler curve of the multicomponent inorganic/organic droplet, which characterizes the variation in equilibrium droplet size with relative humidity, can be determined directly. The measurements presented here focus on high relative humidities, above 97%, in the limit of dilute solutes. The experimental data are compared with theoretical treatments that, while ignoring the interactions between the inorganic and organic components, are based upon accurate representations of the activity-concentration relationships of aqueous solutions of the individual salts. The organic component is treated by a parametrized fit to experimental data or by the UNIFAC model and the water activity of the equilibrium solution droplet is calculated using the approach suggested by Clegg, Seinfeld and Brimblecombe or the Zdanovskii−Stokes−Robinson approximation. It is shown that such an experimental strategy, comparing directly droplets of different composition, enables highly accurate measurements of the hygroscopic properties, allowing the theoretical treatments to be rigorously tested. Typical deviations of the experimental measurements from theoretical predictions are shown to be around 1% in equilibrium size, comparable to the variation between the theoretical frameworks considered.

I. Introduction

Knowledge of the solution thermodynamics governing aerosol hygroscopicity is of considerable importance for understanding the partitioning of water between the gas and condensed phases in atmospheric aerosol. A change in the activity of water in the gas phase must be matched by a corresponding change in the condensed phase for the gas−liquid equilibrium to be maintained.[1,2] As a consequence, solution thermodynamics are key to interpreting the change in cloud droplet size distributions with change in relative humidity (RH) and the hygroscopicity of aerosol is central to understanding the activation of cloud condensation nuclei.[3] Thus, predicting the gas−liquid partitioning of water is crucial for interpreting the influence of aerosols on the properties of clouds, and this is central to resolving the uncertainties surrounding the impact of aerosol on climate. [4]

While the hygroscopic properties of typical inorganic solutes, such as sodium chloride (SC) and ammonium sulfate (AS), are well understood through bulk solution and aerosol measurements, many uncertainties remain in predicting the influence of organic components on aerosol hygroscopicity.[3,5,6] This is partly due to the complexity of the organic mass fraction and the challenges associated with quantifying even the dominant organic components.[7,8] Although it is now recognized that 20−70% of the total particulate carbon in the atmosphere is water soluble,[7] incorporating organic components in thermodynamic models remains challenging.[9] A thermodynamic treatment should include the nonideality of aqueous solutions, incorporating the interactions between the organic and inorganic solutes and their influence on activities where known.[9,10] This becomes particularly important at the high solute concentrations/low RHs that are characteristic of supersaturated solutions.[6,9] The solubility of the organic component in the aqueous phase may be such that immiscible hydrophobic and hydrophilic phases form. As a consequence, it is necessary to consider phase partitioning between the gas phase and discrete aqueous and organic phases.[5,11] Further, the impact of the dissociation equilibria of organic components should be included in the thermodynamic treatment if the mass fraction of the organic components are high with respect to inorganic components, and if the dissociation constants are large enough that the mole fractions of the dissociated species are significant.[12,13] For example, the acid−base equilibria of dicarboxylic acids can affect the pH of aerosols, altering the partitioning of volatile components, such as ammonia and nitric acid, between the gas and condensed phases and thus influencing the partitioning of water.[12]

The vapor pressure and equilibrium size of a solution droplet are influenced by surface curvature as well as solution thermo-

[⊥] Part of the "Stephen R. Leone Festschrift".

* To whom correspondence should be addressed. E-mail: j.p.reid@bristol.ac.uk.

[†] University of Bristol.

[‡] University of East Anglia.

[§] University of Manchester.

10.1021/jp802520d CCC: $40.75
Published on Web 07/02/2008

dynamics. Köhler theory incorporates both of these effects, with the role of solution thermodynamics governed by a solute term and the surface curvature effect governed by a Kelvin term.[2,3] Calculation of the Kelvin term, which reflects the fractional increase in vapor pressure of a curved surface over that of a flat surface, requires knowledge of the surface composition and this is dependent on the surface activity of the organic components, which can be related to surface tension.[14] Further, the surface composition is expected to have an influence on the kinetics of mass transfer between the gas and liquid phases.[15] Both water soluble and insoluble organic compounds may have an impact on the evaporation or condensation rates of water,[16,17] and it has been suggested that this could complicate the measurement of aerosol hygroscopicity.[18]

To fully interpret the influence of organic components on the hygroscopic properties of aerosol, it is necessary to examine the variation in wet particle size over a wide range of RH, to characterize the partitioning of components between immiscible organic and aqueous phases, to probe surface composition and the influence of surface activity on wet particle size, and to ensure that the recorded size is not determined by kinetic limitations to mass transfer. We have recently reported a direct strategy for comparing in situ the variation in wet particle size of two droplets (2−8 μm radius) of differing composition using aerosol optical tweezers.[19] The size of each droplet can be determined with nanometre accuracy and with high time-resolution, <1 s. Further, if one of the droplets is an aqueous solution of a typical inorganic electrolyte, such as SC or AS, the RH can be determined with an accuracy $<\pm 0.09\%$. Using this approach, we have demonstrated that a Köhler curve can be measured with high accuracy at RHs approaching 100%. Further, we have demonstrated that the Raman fingerprint from a trapped droplet can be used to examine the phase segregation of immiscible liquid phases within a single particle,[20] to determine the thickness of an organic film with nanometre accuracy,[21] and to examine crystallization and the formation of metastable gel phases at low RH.[22]

In this publication, we use aerosol optical tweezers to explore the hygroscopic properties of aqueous droplets containing SC, AS and glutaric acid (GA, $C_5H_8O_4$) with varying organic mass fraction. GA is chosen as a representative water soluble dicarboxylic acid. The pure solid has a vapor pressure of $(18.7 \pm 5.9) \times 10^{-5}$ Pa at 298 K and a water solubility of 1.6 kg per kg of water.[23,24] SC and AS are chosen because the thermodynamic properties of their aqueous solutions are well understood.[1,25] The objective of this work is to demonstrate that we can rigorously intercompare the thermodynamic properties of two droplets of different composition using aerosol optical tweezers. More specifically, we will evaluate different thermodynamic models for predicting the variation in wet particle size with RH for mixed GA/SC and GA/AS aqueous droplets and assess the accuracy of the optical tweezers strategy for performing equilibrium size measurements. We will also compare our measurements to previous measurements of the hygroscopicity of mixed component GA/SC and GA/AS aerosol. Previous studies have been made on single particles using electrostatic trapping,[15,26] optical levitation,[27] and droplets immobilized on a hydrophobic surface,[28,29] and in aerosol ensembles using tandem differential mobility analysers.[30,31] The experimental strategy is first outlined in Section II before considering the thermodynamic models used to interpret the experimental data in Section III. This is followed in Section IV by a study of the hygroscopic properties of mixed GA/SC and GA/AS aqueous droplets, comparison of the experimental data with theoretical models, and an evaluation of the accuracy of the aerosol optical tweezing technique for performing such measurements.

II. Experimental Technique

The aerosol optical tweezers technique and the spectroscopic characterization of trapped droplets have been discussed in detail in previous publications[19,32] and will only be described briefly here. Light from a Nd:YVO_4 laser operating at 532 nm is focused through a 100× oil immersion objective (NA 1.25) into a custom fabricated cell, which allows control of the gas phase composition. The light comes to a tight focus ~40 μm above the microscope coverslip, exerting a strong gradient force on any aerosol particle that drifts into the focal volume.[33] Aerosol is introduced into the cell from an ultrasonic medical nebulizer (Omron NE-U07) and any droplets passing near the laser beam focus are drawn to the focus of the light and captured. The composition of the captured droplets has been shown to be identical to that of the nebulized solution.[19] As the aerosol plume subsides, growth of the trapped droplet can occur through coagulation with other aerosol droplets. In the experiments described here, the optical design includes a beam-splitter which divides the laser beam and forms two optical traps that can be independently controlled.[19] One trap is first loaded with an aqueous droplet containing the organic component GA and the second trap is then loaded with an aqueous droplet containing either SC or AS. During this second step, some inorganic solute is added to the organic doped droplet by coagulation, forming a mixed inorganic/organic aqueous droplet.

The droplets are imaged by conventional brightfield microscopy, using a blue LED centered at 450 nm as the illumination source.[32] Raman scatter is collected in the backscattering direction by collimation of the Raman light through the microscope objective. The red Raman light is separated from the green and blue light used for trapping and imaging by appropriate filters and dichroics. The Raman light is focused into a 0.5 m focal length spectrograph equipped with a 1200 g/mm grating and a CCD array of 1024 × 256 pixels allowing acquisition of the entire dispersed Raman fingerprint with 1 s time-resolution. To acquire the spectra of two droplets, the droplets are sequentially steered to a point in the trapping region that is preferentially aligned to the optical axis of the spectrograph.

The Raman spectra consist of an underlying spontaneous Raman scattering band, Stokes shifted from the excitation laser wavelength of 532 nm, with superimposed resonant structure arising from enhancement of the Raman scatter at wavelengths commensurate with whispering gallery modes (WGMs).[32,34] An example of the evolving Raman fingerprint of an aqueous SC droplet, in particular the varying wavelengths of the WGMs, is shown in Figure 1. Spontaneous Raman scatter arises from excitation of the OH stretching vibrations of water and is observed as a broadband extending from ~635 to 660 nm, a Stokes shift of between 3050 and 3650 cm^{-1}. The wavelengths of the WGMs that occur within the spontaneous band envelope allow the size of the droplet to be determined with nanometre accuracy, dependent on the accuracy with which the refractive index of the droplet is known.[35] The method for treating the refractive indices of droplets containing SC, AS and GA has already been discussed.[19] In the measurements presented here, the evolving wet particle size of the inorganic solute droplet, referred to as the control droplet, is used to determine the changing RH with time. From simultaneous measurements of the wet particle size of the inorganic/organic droplet, referred to as the multicomponent droplet, the Köhler curve of this droplet can be determined directly.

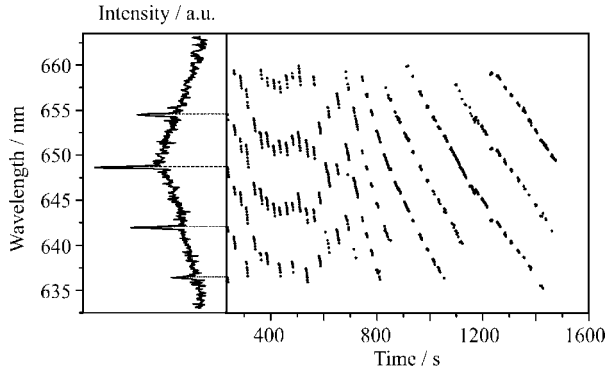

Figure 1. Illustration of the form of the experimental data. The left panel shows the Raman spectrum of an aqueous SC droplet in the OH excitation region. The right panel shows the time evolution of the wavelengths of the WGM resonant modes on the OH band for this droplet. Gaps in the time dependence occur at times when the spectrum of the second droplet, the multicomponent droplet, is acquired.

III. Thermodynamic Models

The radii measured from the pair of droplets can ultimately be expressed as the variation of the radius of the multicomponent droplet with RH. This variation can be compared with predictions from Köhler theory[9,36] or with growth factor parametrizations of experimental data available from the literature.[24,30,37] We now consider the specific droplet properties that must be understood and incorporated in the theoretical models in order to interpret the measurements.

Köhler theory accounts for the contributions of the solute and Kelvin effects to the variation in equilibrium droplet size with RH, and can be expressed as

$$RH = a_w \exp\left(\frac{2V_w\sigma}{RTR_p}\right) \quad (1)$$

where a_w is the activity of water in an equivalent bulk solution with the same solute molality as the droplet, V_w is the partial molar volume of water, σ is the surface tension of the solution, R_p is the radius of the liquid droplet, and R and T are the ideal gas constant and the temperature. The calculation of changes in droplet size with RH requires a knowledge of three quantities: the water activity, the partial molar volume, and the surface tension of the droplet and their dependence on solution concentration. It should be noted that although the concentration of an involatile solute varies with RH, the solute mass is invariant and is often expressed as an equivalent dry particle size. In the limit of large droplet size, equation 1 reduces to $RH \sim a_w$, reflecting the declining influence of surface curvature with increasing droplet size and leading to a simple dependence of the vapor pressure of the droplet on the activity of water in the solution. The calculations of droplet water activity, density, and surface tension are described below. The reader should refer to the Appendix for details of the computer codes used.

a. Water Activity. Water activities of pure aqueous solutions of glutaric acid,[9] sodium chloride,[38] and ammonium sulfate[39] are well established. Some data are available for mixtures of glutaric acid and the two salts (see Table 8 of ref 9), mostly for concentrated solutions. At the high RH studied here, mixture effects should be small and we have therefore calculated water activities using two alternative methods that require only information for the water activity/concentration relationships of the pure aqueous solutions (of the acid, and of the salt). The relationships between solution molality and water activity for aqueous SC and AS were calculated using the equations and parameters given by Clegg et al.[1] For aqueous GA, the relationship between solution molality and water activity was either calculated using UNIFAC[40] with the modified parameters proposed by Peng et al.[41] or an equation directly fitted to water activity data.[9] The two alternative methods with which the water activities of the mixed solution droplets were estimated are summarized below.

i. Zdanovskii-Stokes-Robinson (ZSR). The ZSR relationship[42] states that, for a specified water activity (a_w), the total water content (W_{total}) of an aqueous solution containing two dissolved solutes can be expressed as:

$$W_{\text{total}} = w_a^{\,o} + w_b^{\,o} \quad (2)$$

where $w_a^{\,o}$ and $w_b^{\,o}$ are the amounts of water associated with the two solutes a and b in pure aqueous solutions at the same water activity as the mixture. The expression can be generalized to an arbitrary number of solutes, thus $W_{\text{total}} = \Sigma_i\, w_i^{\,o}$. The ZSR approach can be expanded to incorporate interaction terms using additional parameters and also unsymmetrical effects for mixtures containing solutes of different charge types (such as the mixtures studied here).[43] Here we use it in its simplest form, expressed by eq 2, as the mixture effects are small at the high RH used in the experiments. The calculations of droplet size made using this method were carried out with the model ADDEM,[2,36] and incorporate the surface curvature (Kelvin) effect described by eq 1. Further details of the model are provided in the Appendix, section B.

ii. Clegg, Seinfeld and Brimblecombe (CSB). These authors have proposed a thermodynamically self-consistent method for estimating solvent and solute activities in solutions containing both ionic and (uncharged) organic components.[11] In this method the activity of water, a_w, in the mixture is given by

$$a_w = a_w(\text{I}) \times a_w(\text{O}) \quad (3)$$

where a_w(I) is the water activity calculated for a solution containing the total amount of solvent and the ionic solutes in the mixture, and a_w(O) is the water activity calculated for a solution containing the same amount of solvent plus the uncharged organic solutes. There are corresponding expressions for the activity coefficients, γ_i, of the solute species.[11] The CSB method is equivalent to using a molality-based activity coefficient model such as that of Pitzer[44] but without parameters for interactions between ionic and uncharged solutes, which in many cases are unknown.

Water activities estimated using the CSB approach, and based upon a_w(O) of pure aqueous GA fitted to measured values at room temperature, are referred to as CSB-Fit. Water activities which use UNIFAC predictions for the pure aqueous acid are referred to as CSB-Peng. The calculations of droplet size based on these water activities, which were carried out using the extended aerosol inorganics model (E-AIM) of Wexler and Clegg,[45] do not include the Kelvin effect described by eq 1. Further details of the model are provided in the Appendix, section A.

b. Solution density. In order to calculate the radius and partial molar volume of water in eq 1, the density of the solution droplet must be estimated. This is done using the following rule:[46]

$$\frac{1}{\rho_{sol}} = \sum_i \frac{X_i}{\rho_{oi}} \quad (4)$$

where X_i is the dry solute mass fraction of compound i, and ρ_{oi} is the density of a pure aqueous solution of compound i at the

TABLE 1: Solid Densities and Parameters for Growth Factor Treatment[30,37]

system parameter	sodium chloride	ammonium sulfate	glutaric acid
density of solid/(g cm^{-3})	2.165	1.769	1.424
	Growth Parametrization		
a	4.83257	2.42848	0.99597
b	−6.92329	−3.85261	2.34929
c	3.27805	1.88159	1.58981

same water activity as the mixed solution. For the two inorganic salts the equations of Tang relating solution density to solute mass fraction were used.[46] For aqueous solutions of GA, densities were calculated using pure compound densities and the ideal mixture theory following Gaman et al.[47]

c. Surface Tension. Measured surface tensions are available for many aqueous inorganic solutions and a number of aqueous organic solutions, but an estimation method is generally required for mixtures.[14] The simplest approach is to add contributions calculated for the individual compounds and salts present in the mixture. Here, the deviations from the surface tension of pure water for aqueous GA and aqueous salt solutions are added to the value for pure water to obtain an estimate for the mixture:

$$\sigma_{ws} = \sigma_w + \Delta\sigma_{org} + \Delta\sigma_{inorg} \quad (5)$$

where σ_w is the surface tension of pure water at the temperature of interest, and $\Delta\sigma_{org}$ and $\Delta\sigma_{inorg}$ are differences between σ_w and the surface tensions of aqueous solutions of the organic acid (σ_{org}) and inorganic salt (σ_{inorg}) at the same molality as in the mixture. Thus, $\Delta\sigma_{inorg}$ is equal to $\sigma_{inorg} - \sigma_w$, and $\Delta\sigma_{org}$ is equal to $\sigma_{org} - \sigma_w$.

In our calculations both $\Delta\sigma_{org}$ and $\Delta\sigma_{inorg}$ are based on measured surface tensions. For aqueous GA we used experimental data within the method of Li and Lu[48] as described by Topping et al.,[14] to provide a continuous set of values derived from a sparse set of experimental data points. For the inorganic salts we used the fitted equations of Chen et al.;[49] see ref 14 for details.

d. Growth Factor Treatment. A growth factor is a convenient parameter for describing the hygroscopic properties of aerosol,[37] and is defined as the ratio of the wet particle diameter at a specified RH, *d*(*RH,wet*), to the dry particle diameter, *d*(*dry*).

$$GF(RH) = \frac{d(RH, wet)}{d(dry)} \quad (6)$$

The growth factor is determined at varying RHs to fully characterize the hygroscopicity of the aerosol. Growth measurements have been made for GA/AS particles[30,31] at RHs up to 95% and for GA/SC particles[31] up to 85% RH using humidified tandem differential mobility analysers. Single particle growth factor measurements have also been published for GA/AS and GA/SC using electrostatic trapping up to 80% RH.[26] Kreidenweis et al.[37] have derived and evaluated a parametrization of the RH dependence of the GF for SC and AS and Prenni et al. and Koehler et al. have provided similar data for GA.[24,30] These parametrizations, referred to as the growth factor parametrization (GFP) treatment, are based on a polynomial fit to the growth factor data of the form

$$GF(\mathrm{RH}) = \left[1 + (a + b\mathrm{RH} + c\mathrm{RH}^2)\frac{\mathrm{RH}}{1 - \mathrm{RH}}\right]^{1/3} \quad (7)$$

In this equation, the RH is the relative humidity expressed as a fraction with 1 equivalent to saturation. The coefficients *a*, *b* and *c* are given in Table 1 and the values account for corrections to remove the Kelvin dependence of the growth factor.[37] Although this study aims to examine the consistency and accuracy of the different modeling approaches (both versions of CSB within E-AIM, and ZSR within ADDEM including ρ_{sol} and σ_{ws}, as described in Sections III.a–IIIc), the GFP treatment is included as this has already formed the basis for our previous benchmarking study and provides a convenient and straightforward parametrization for providing a first analysis of the experimental data.[19]

From the initial size of the trapped droplets, the mass of each solute can be calculated and converted into a dry particle size, assuming the solid densities in Table 1. This is based on an assumption that the initial composition of the aerosol is the same as that of the solution prior to nebulization; this has been confirmed by measurements of the refractive index of the delivered aerosol. Thus, the wet particle size can be calculated for pure SC or GA droplets at any RH. Then, for the size of the mixed component droplet, the ZSR approximation is assumed. The wet particle size and volume of water associated with each component are each estimated independently and, thus, the total volume of the mixed droplet.[24,30]

e. Comparison of Predictions from Theoretical Models. We compare predictions of growth factors from three theoretical treatments (CSB-Fit, ADDEM and GFP) in panels a and b of Figure 2 for binary and ternary component droplets, respectively, over the RH range relevant to our experiments, above 97%. A comparison of these three treatments is crucial to interpret the experimental data correctly. Further, the CSF-Fit, CSB-Peng and ADDEM models are compared over the wider RH range down to 50% in Table 2 for mixed component GA/SC and GA/AS droplets. It is important to stress that a ±1 nm accuracy in the size determination, typical of the experiments presented here, corresponds to a percentage error in the growth factor of <0.1% for droplet sizes of greater than 3 μm.

The growth factors for binary component SC and AS droplets are in excellent agreement when predictions from the CSB and ADDEM are compared (Figure 2a), consistent with the underlying treatment of the electrolyte solution thermodynamics. It is also significant that the growth factor at the highest RH calculated from ADDEM is smaller by 0.03 than the predictions from CSB for both the SC and AS systems. This is consistent with the inclusion of the surface curvature term in the calculation of the equilibrium size from ADDEM and has a significant impact on the predictions as saturation is approached, elevating the equilibrium RH at a particular droplet size. This difference decreases to ~0.01 at the lowest RH shown in the figure of 97%. The growth factor calculated by the GFP method is marginally lower than both treatments for SC and AS, and this is qualitatively consistent with the comparison made by Kreidenweis et al.[37] The maximum deviation of GFP from CSB-Fit is −1.6% and −4.1% for the SC and AS systems, respectively.

The growth factors for GA are again in good agreement from both CSB-Fit and ADDEM predictions, although a small deviation of ADDEM from the CSB-Fit of 2.5% does emerge at the lowest RHs examined here, reflecting the differences between the underlying treatments of the water and organic component activities. This is consistent with an overestimate of the growth factor when treating the organic component within the UNIFAC framework. These differences become smaller at the highest RH, though the apparently complete agreement at 99% RH is partly fortuitous given that the ADDEM prediction also incorporates a surface tension term. Predictions from the GFP are consistently higher than from CSB-Fit and ADDEM

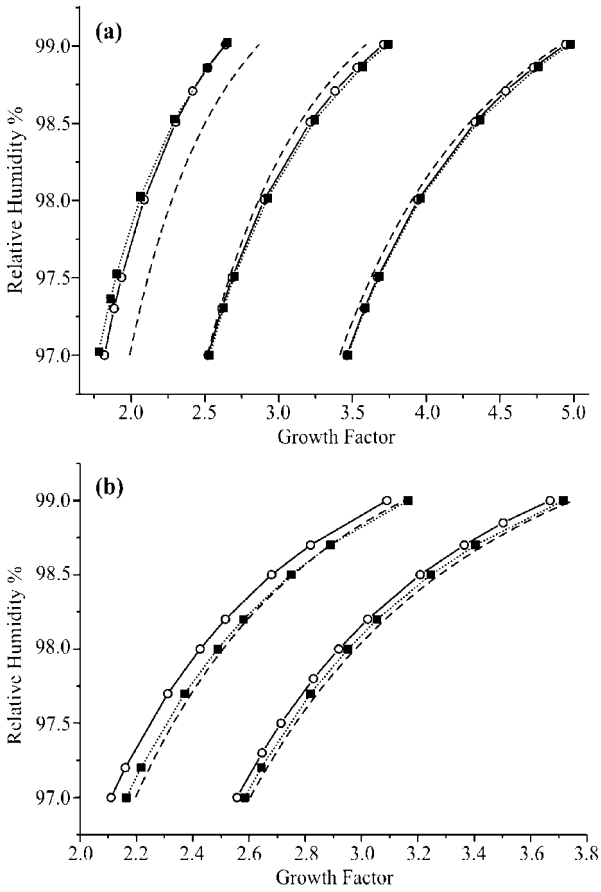

Figure 2. (a) Comparison of model predictions (solid line and open circles: ADDEM; dotted line and filled squares: CSB-Fit; dashed line GFP) for the growth factors of GA, AS and SC (left to right) over the RH range of the measurements. (b) Comparison of model predictions (solid line and circles: ADDEM; dotted line and squares: CSB-Fit; dashed line GFP) for multicomponent GA/AS (left) and GA/SC (right) droplets For the GA/SC droplet, the GA/SC mass ratio is 1.506, a molar ratio 0.667, and the dry particle size is 1283 nm. For the GA/AS droplet, the GA/AS mass ratio is 1.573, a molar ratio 1.572, and the dry particle size is 1720 nm.

with a percentage deviation of 12% from the former at the lowest RH. This is again qualitatively consistent with a previous comparison of this treatment with predictions from Clegg.[24]

Table 2 and Figure 2b compare the difference in growth factors and wet particle sizes for mixed component droplets of GA/SC and GA/AS with mass ratios of 1.506:1 (a molar ratio of 0.667) and 1.573:1 (a molar ratio of 1.572), respectively, typical of the measurements that will be presented. The difference between ADDEM and CSB varies with RH, not just in magnitude but in sign: above about 90% RH ADDEM gives more concentrated, smaller, droplets. In this range (90−100% RH) the maximum difference between the two treatments occurs at about 94% RH and these differences can be shown to be consistent with differences arising from the underlying treatment of the water activity of the solution droplet within the CSB and ZSR frameworks and the inclusion of surface tension in the ADDEM calculations.

Below 90%, ADDEM predicts larger, more dilute droplets than the CSB treatment. By 80% the ADDEM prediction is larger than that from both CSB-Fit or CSB-Peng by 20−40 nm, a percentage difference of less than 2.5%. This difference persists to the lowest RH examined of 50%. Further, differences between the CSB-Fit and CSB-Peng treatments are quite small, as seen in Table 2, supporting the conclusion that UNIFAC

TABLE 2: Comparison of Total Solute Molalities and Wet Particle Radii Calculated with the ADDEM, CSB-Fit and CSB-Peng Approaches over the RH Range of 0.5−0.99 for GA/SC and GA/AS Droplets[a]

	total solute molality (GA + salt)/mol kg^{-1}			equilibrium wet particle radius/μm		
RH	ADDEM	CSB-Fit	CSB-Peng	ADDEM	CSB-Fit	CSB-Peng
			Sodium Chloride/Glutaric Acid System			
99	0.390	0.371	0.367	4.707	4.769	4.772
98	0.789	0.753	0.745	3.745	3.787	3.792
97	1.20	1.14	1.13	3.281	3.316	3.322
97	3.91	3.85	3.79	2.303	2.300	2.308
80	7.22	7.48	7.37	1.962	1.938	1.944
70	10.3	10.8	10.7	1.809	1.778	1.781
60	13.4	14.1	14.0	1.714	1.678	1.680
50	16.8	17.6	17.5	1.645	1.606	1.607
			Ammonium Sulfate/Glutaric Acid System			
99	0.410	0.379	0.362	5.321	5.450	5.459
98	0.877	0.793	0.772	4.177	4.284	4.299
97	1.39	1.23	1.21	3.633	3.727	3.746
90	5.11	5.09	4.80	2.558	2.566	2.588
80	9.88	10.6	10.4	2.238	2.216	2.224
70	14.7	15.8	15.8	2.102	2.075	2.076
60	20.3	21.4	21.4	2.017	1.988	1.987
50	27.4	27.9	27.9	1.955	1.924	1.924

[a] For the GA/SC droplet, the GA/SC mass ratio is 1.506, a molar ratio 0.667, and the dry particle size is 1283 nm. For the GA/AS droplet, the GA/AS mass ratio is 1.573, a molar ratio 1.572, and the dry particle size is 1720 nm.

model quite closely represents the measured activity-concentration dependence for this acid. A previous application of a ZSR-based model to experimental water activity measurements for both GA/AS and GA/SC solutions over an extended RH range has shown that a salt-acid interaction parameter is required to represent the data accurately.[9] The influence of this parameter decreases as the solution becomes more dilute, and has therefore not been included in the calculations in this work where we model the experimental data. The values of droplet molality and size in Table 2, calculated without salt-acid interaction parameters in either model over an extended RH range, are representative of the general differences between the models, but are unlikely to be accurate at the lowest RHs.

IV. Experimental Measurements of Hygroscopicity

In previous work we have demonstrated that an intercomparison of two trapped droplets of SC can provide a highly accurate strategy for comparing the hygroscopicity of two droplets, with the wet droplet sizes determined with nanometre accuracy and the RH determined from the control droplet with an accuracy better than ±0.09%.[19] A preliminary experiment on one GA/SC aerosol droplet was presented in this earlier paper based on the GFP treatment. This strategy is now used to investigate the impact of GA on the hygroscopicity of SC or AS aerosol with varying organic mass fraction.

The evolving radii of two aqueous droplets are shown in Figure 3a. In this measurement, a GA droplet, with an organic solute concentration of 50 g/L, was first captured in one optical trap. The initial size of this droplet was used to determine the mass of GA in the droplet. The second trap was then loaded with a SC control droplet with a solute concentration of 20 g/L. Again, the initial size of this droplet was used to determine the mass of SC in the droplet. The initial size of the control droplet was 4.496 μm which is equivalent to a SC mass loading of 7.56 pg and an equivalent dry (spherical) particle size of 0.943

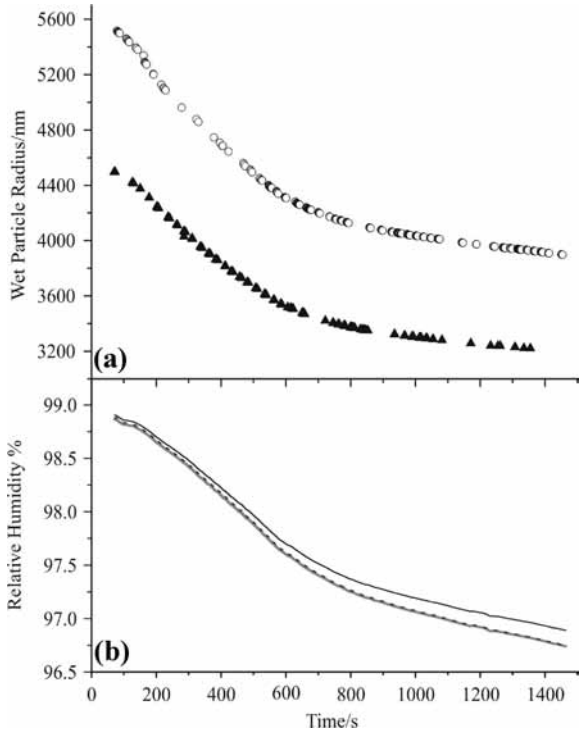

Figure 3. (a) Time dependencies of the wet particle size of a GA/SC droplet (circles) and a SC control droplet (triangles). (b) Estimated RH determined from the evolving size of the SC control droplet calculated from ADDEM (solid gray line), CSB-Fit (dashed black line) and GFP (solid black line). The ADDEM and CSB-Fit models show excellent agreement while the GFP leads to an overestimation of the RH.

μm. To convert the evolving size of the control droplet into a measurement of RH, the mass of SC in this droplet (or alternatively the dry particle size) was used to predict the variation in wet particle size with RH using the CSB-Fit, ADDEM and GFP models. The time dependence of the size was then used directly to determine the time dependence of the RH. The RHs estimated from these three theoretical treatments are compared in Figure 3 and, as expected from the similarity of the growth curves in Figure 2, the agreement is excellent, particularly between the RH estimates from ADDEM and CSB-Fit with a maximum difference of only 0.006%. The largest difference in the comparison between RHs determined from CSB-Fit and GFP is 0.15%, reflecting the differences in growth factors between these treatments presented in Figure 2a. Further, the time variation in RH shown in Figure 3b clearly illustrates the precision with which the RH can be followed. In all subsequent measurements, consistency is maintained between the model used to estimate the RH and the model used to predict the Köhler curve for the multicomponent droplet.

When loading the control droplet into the second trap, the GA droplet was observed to grow by coagulation with SC aerosol forming a multicomponent droplet containing GA and SC. In order to compare the measured Köhler curve for this droplet with model predictions, it is essential to know the additional solute mass added to the droplet during this step. However, the size change arises from both a RH change and coagulation. Introduction of a SC aerosol flow into the cell changes the RH inducing a size change in the GA droplet, as illustrated by the schematic in Figure 4. In this particular study, the well-characterized solution thermodynamics allow the size change accompanying the RH change to be estimated with high accuracy for the GA droplet. It is then possible to establish

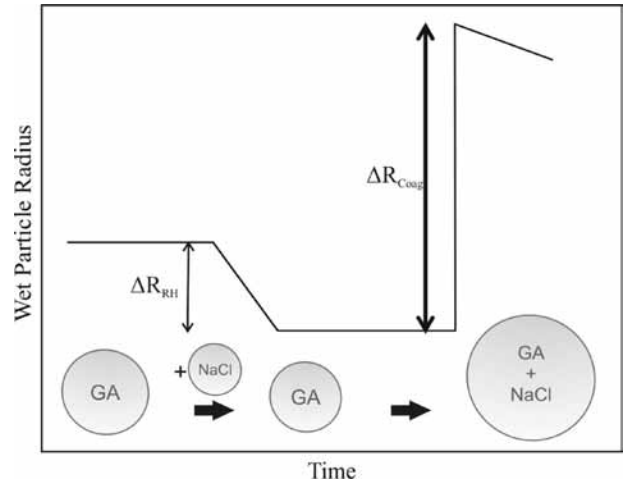

Figure 4. Schematic illustrating that the size change of the multicomponent droplet must be resolved into (1) a size change due to a RH change, ΔR_{RH}, as the SC aerosol flow is introduced, and (2) a size change due to coagulation with the SC aerosol flow, ΔR_{Coag}. Both must be included in the analysis to correctly determine the amount of the inorganic solute added to the multicomponent droplet.

accurately the size change due to coagulation to estimate the SC mass added to the droplet.

One cautionary point should be noted when considering the accuracy with which the size of the droplet following coagulation is known. The accuracy of the size is dependent on knowing the composition and, thus, refractive index of the droplet. However, to estimate the compositional change the size change must be known, a seemingly circular requirement. To circumvent this, the multicomponent droplet size is first estimated using the refractive index of the initial GA solution, providing a first estimate of the new composition. This can then allow an estimation of the size change and hence compositional and refractive index changes. A second iteration on the fit of the size at the refined refractive index then provides a more accurate estimation of the new size. This process can be repeated to iteratively improve the size and compositional analysis. In these experiments, it is not necessary to go beyond one iteration to improve the accuracy on the size, mainly because the dependence of the error incurred in fitting the size is not significantly influenced by the uncertainty in refractive index. This is illustrated in Figure 5. Even an error of 100% in the concentration of either solute leads only to an error in the wet droplet radius of ~12 nm or, typically, ~0.25%. This translates to an error in the corresponding dry particle diameter of typically ~2 nm for dry solute particles typically larger than 1 μm in diameter. All subsequent wet and dry particle sizes should be assumed to be accompanied by a $\pm$1 nm error.[19]

For the data set shown in Figure 3, the initial pure GA droplet had a wet size of 3.979 μm and thus a GA mass loading of 13.2 pg and a dry particle radius of 1.30 μm. At a RH of 98.90%, subsequent to loading the control droplet, the multicomponent droplet grew to 5.517 μm. It is first necessary to estimate the size change arising from the RH change alone, before estimating the mass of SC added to the droplet by coagulation. The equilibrium wet radius for the GA droplet at a RH of 98.90% can be estimated to be 3.201 μm. Thus, introducing the flow of SC aerosol leads to a decrease in the RH and a decrease in the equilibrium size of the pure GA droplet. Eventually, as a result of coagulation with SC aerosol, the wet particle radius increased to 5.517 μm. Thus, the size increase due to coagulation equates to the addition of 11.2 pg of SC to the droplet.

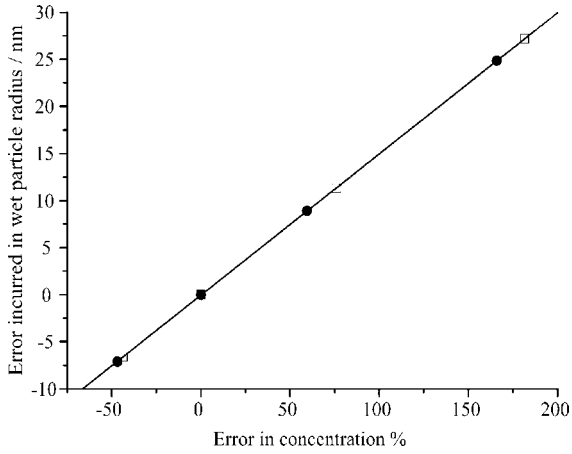

Figure 5. Error incurred in the size determination of the multicomponent droplet with percentage error in the solute concentration (squares, SC solute; circles, GA solute). The errors remain small even with large uncertainties in the solute concentration due to the dominance of the water component in determining the refractive index.

To illustrate the importance of accounting fully for the compositional changes, three treatments of the composition and refractive index are compared in Figure 6. If it is assumed that no additional solute is added to the GA droplet through coagulation with SC aerosol, the Köhler curve predicted from the GA mass alone is an underestimate of that measured experimentally by ~1.5 μm. If the size change of the GA droplet is assumed to result from coagulation with SC alone, the estimated SC mass added is insufficient to increase the predicted wet particle size to that observed. Only when the decrease in size accompanying the RH change is included, along with growth by coagulation, is the added SC mass sufficient that the measurement and prediction are consistent. The GFP is used in this figure as this effect is independent of the treatment used. This also allows the reader to examine directly the dependence of the Köhler curve on the treatment used, by comparison of Figure 6 with Figure 7.

The dependence of the calculated multicomponent droplet size on the method for treating the refractive index is considered in Figure 6b. If the refractive index of the multicomponent solution is assumed to remain that of the original GA solution, the error incurred in the size when compared to a full iterative treatment of refractive index is <1 nm. If the influence of the change in RH is not included in the estimate of compositional change, the calculated droplet size is ~3 nm larger than that from the full treatment.

To illustrate the contributions of the organic and inorganic components to the equilibrium size, the wet droplet sizes that would be associated with the aqueous GA and SC volume fractions alone are shown in Figure 7, along with the combined wet droplet size. The dominance of the contribution from the inorganic component is clear, even though the organic component represents a larger solute mass fraction. The mean difference between experiment and theory is +5 nm over the RH range 98.8−96.8% with a standard deviation of ±30 nm, reflecting the fact that the measured size is larger than theory (ADDEM) by ~85 nm at high RH and smaller at low RH by ~15 nm. These differences are summarized in Table 3 as errors in growth factors, principally to allow direct comparison with TDMA and EDB data that span the range from particles 100 nm in diameter to 50 μm.

A similar level of agreement is observed when the experimental analysis and theoretical prediction are undertaken with

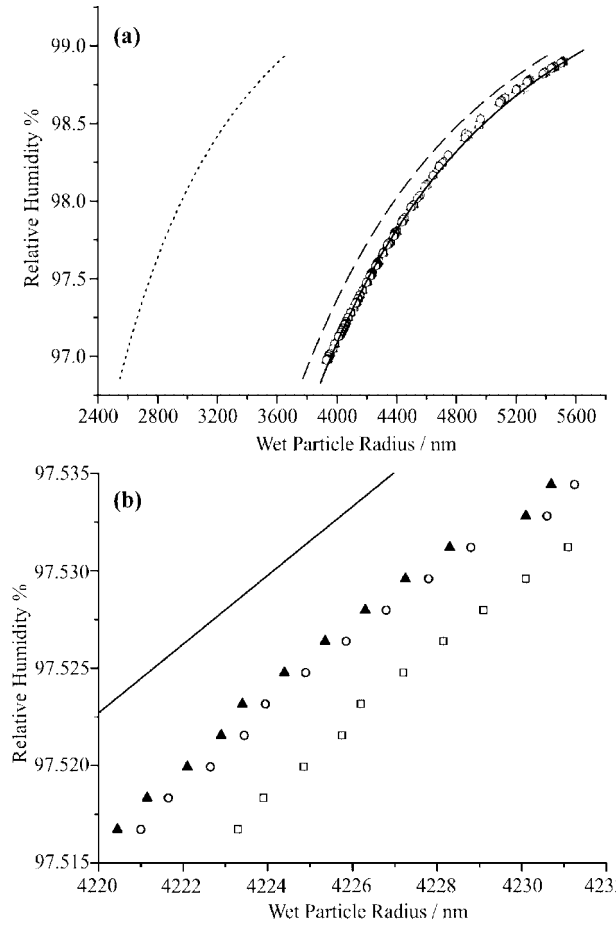

Figure 6. (a) Illustration of the need to include the compositional change in the multicomponent droplet arising from RH and coagulation changes when loading the control droplet. If the RH change is considered alone with no additional inorganic solute added, the theoretical prediction resulting is shown by the dotted line. If the RH change is neglected and the size change is attributed solely to coagulation, the dashed line prediction results. Only if both are included are the measured and predicted sizes consistent. The theory used in this analysis is the GFP, illustrating the good agreement achieved providing a consistent treatment is used for both droplets. (b) Expanded region with the solid line representing the predictions and different refractive index treatments for the experimental analysis: triangles - sizes if the refractive index of the multicomponent droplet is assumed to remain that of the GA solution; squares, sizes if the change in RH is not included in the estimate of compositional change; circles, incorporating the full treatment of refractive index.

the CSB-Fit treatment. A comparison between experiment and CSB-Fit shows that the experimental size is too small at high RH and too large at low RH, both by ~50 nm, ~1% of the size. By contrast, the GFP prediction is consistently larger than the measurement by ~30 nm. From this comparison it is clear that the level of agreement between experiment and prediction is similar for all three possible treatments of the data, provided that both the SC and the GA/SC droplets are treated within the same model framework. This is unlikely to remain true if the organic component were dominant in determining the wet particle size or if the solutions were to depart from ideality. This latter condition is particularly relevant at low RH and high solute concentrations, conditions at which some of the fundamental assumptions made within the models will be rigorously tested.

Comparisons between further measurements and predictions for a range of GA/SC and GA/AS droplets of varying mass ratios are presented in Figure 8, analyzed using ADDEM. In

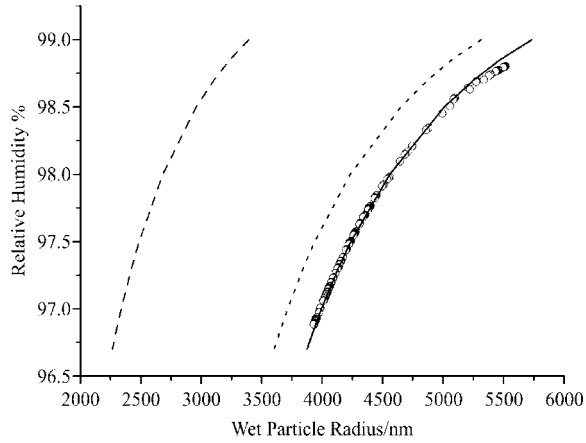

Figure 7. Comparison of the measurements (circles) and predictions (solid line) for the droplet shown in Figure 4, using the ADDEM treatment. The predictions arising for the GA (left dashed line) and SC (right dashed line) components alone are shown for comparison.

the experiments involving AS, the RH was determined from an AS control droplet in an analogous manner to the measurements using a SC control droplet. A comparison of the mean differences in GFs between the measurements and ADDEM predictions for these systems is summarized in Table 3. The agreement is excellent for all organic/inorganic mass ratios studied and no systematic dependence in the agreement with organic mass fraction is observed. It should be noted that for all of the experiments performed, the maximum mean difference in the measured wet particle size from ADDEM is $<1\%$ or 30 nm for a 4 μm radius droplet, with many of the measurements yielding errors of $\ll 1\%$ corresponding to only a few nanometers error in size. The data for the GA/AS is consistently lower than the predictions from ADDEM. Further work will need to examine the variation in wet particle size with RH over larger RH ranges to see if this is indicative of a systematic effect not reflected in the model predictions.

The accuracy of the measurements presented here is compared with experimental data recorded in past studies in Figure 9 and Table 3. The extremely accurate nature of these measurements relies substantially on the accuracy of the thermodynamic predictions for the SC or AS aerosol, allowing the calculation of the RH with an accuracy far superior to that achieved in previous measurements. This is reflected by the extremely low values of the mean difference in growth factor between that measured and that predicted from ADDEM. Further, for the mass fractions of the organic component considered here, which lie in a similar range to those previously studied, the inorganic solute component largely dominates the hygroscopicity (Figure 7).

Unlike many of the measurements made by other techniques, the standard deviation of the difference in growth factor between ADDEM and the measurement (also presented in Table 3) is larger than the magnitude of the mean difference, reinforcing the conclusion that the measurements are not only precise but accurate, if ADDEM itself is assumed to provide accurate predictions. This is reinforced by the data shown in Figure 9. It is clear from this figure that the agreement between ADDEM and CSB-Fit is exceptional when compared to the agreement between all previous experimental data and ADDEM, even though the CSB-Fit prediction do not account for the surface curvature term. The agreement between our experimental data and ADDEM approaches this same level of agreement, and should thus allow us to resolve any discrepancies between the different model frameworks. It will be essential to see if this level of accuracy persists even to low RH, under conditions for which the hygroscopic properties of a supersaturated control droplet must be known.

V. Conclusions

Comparative measurements of the hygroscopic properties of inorganic and inorganic/organic aqueous droplets are presented. An aqueous SC or AS of known solute mass loading is used to probe the evolving RH with an accuracy of better than $\pm 0.09\%$ and with 1 s time resolution in close proximity (<50 μm) to a droplet containing GA and either SC or AS. By determining the evolving size of the multicomponent droplet with nanometer accuracy, the Köhler curve can be determined directly and compared with theoretical predictions. Predictions from four models are compared in this work: CSB-Fit, CSB-Peng, ADDEM and GFP, each of which compares well with the experimental data. Errors for the mean deviation between the experimental and theoretical predictions are presented in Table 3. The high accuracy of these measurements compares well with previously benchmarked techniques for determining growth factors and their dependence on RH, as shown in Figure 9.

In this example, it is essential to account for the RH change on introducing the inorganic control aerosol flow and the impact of this on the water activity associated with the organic aerosol component. In future measurements this will be circumvented by first adjusting the RH in the cell to that of the control aerosol flow before introducing the control aerosol. This will allow the size changes of the multicomponent aerosol due to RH change and coagulation to be unambiguously separated, a crucial step when the solution thermodynamics of the organic component are not well characterized.

The versatility of the aerosol optical tweezers approach for probing aerosol dynamics has already been highlighted. This publication provides an important benchmark for testing models such as ADDEM and CSB-Fit and for rigorously assessing these models under the conditions observed at high RH. Although the measurements presented here are performed in the dilute limit that can be accessed through simpler bulk phase studies, this study serves as a first step toward extending the technique into the supersaturated regime at low RH that cannot be accessed in bulk solutions. At low RH, the thermodynamic properties are characterized by nonideal behavior and the interactions between organic and inorganic components must be considered. A further advantage of the comparative optical tweezers approach is that timescales for equilibration in droplet size, the influence of organic films on the rate of size change, and the RH of crystallization for multicomponent droplets can be directly compared.

Appendix

A. Extended Aerosol Inorganics Model (E-AIM). Calculations of water activities (CSB-Fit and CSB-Peng), for the mixed solution droplets, were carried out using the extended aerosol inorganics model (E-AIM) of Wexler and Clegg (http://www.aim.env.uea.ac.uk/aim/aim.php).[25,42] With the RH, temperature and amounts of solute present set as input, an iterative procedure is used to determine the equilibrium state of the system, including the amount of liquid water present. The relationships between solute concentration and water activity for aqueous NaCl and $(NH_4)_2SO_4$ are built into the model, as are both the UNIFAC and fitted equations for aqueous glutaric acid. In E-AIM, the surface curvature effect in eq 1 is neglected

TABLE 3: Comparison of the Accuracies of Experimental Studies on the GA/SC and GA/AS Systems When Compared with Predictions from ADDEM[a]

study	RH range of experimental study	mass fraction of GA, balance SC or AS	growth factor range	mean difference in growth factor from ADDEM	standard deviation of difference
		Sodium Chloride/Glutaric Acid System			
TDMA, Cruz and Pandis[31]	85 ± 1%	0, 0.2, 0.5, 0.8	1.3–2.1	−0.16	±0.10
EDB, Choi and Chan[26]	58 to 80%	0.5	1.38–1.61	+0.051	±0.026
this work	98.6 to 99%	0.32	3.8–4.2	−0.029 (−28 nm)	±0.006
	98.6 to 99%	0.50	3.5–3.9	+0.013 (+14 nm)	±0.010
	97 to 99%	0.54	2.6–3.7	+0.0028 (+4 nm)	±0.020
	98.4 to 99%	0.55	3.2–3.7	+0.0027 (+3 nm)	±0.006
	98.1 to 99%	0.68	2.8–3.4	+0.011 (+13 nm)	±0.008
Ammonium Sulfate/Glutaric Acid System					
TDMA, Cruz and Pandis[31]	85 ± 1%	0, 0.2, 0.5, 0.8	1.2–1.4	−0.11	±0.05
TDMA, Prenni et al.[30]	80 and 90%	0.01, 0.09, 0.4	1.3–1.6	−0.084	±0.010
EDB, Choi and Chan[26]	59 to 80%	0.5	1.02–1.43	+0.0023	±0.081
Bulk, Choi and Chan[26]	80 to 99%	0.5	1.4–3.2	+0.075	±0.021
This work	99.27 to 99.4%	0.83	3.18–3.4	−0.01144 (−16 nm)	±0.00401
	99.35 to 99.4%	0.66	3.56–3.65	−0.01106 (−20 nm)	±0.00186
	99.3 to 99.4%	0.85	3.22–3.37	−0.00233 (−3 nm)	±0.00272

[a] Only tabulated data in previous publications is included in the comparison. In the data presented from this work, equivalent mean errors in radius are also given in brackets for comparison along with the absolute errors in growth factor.

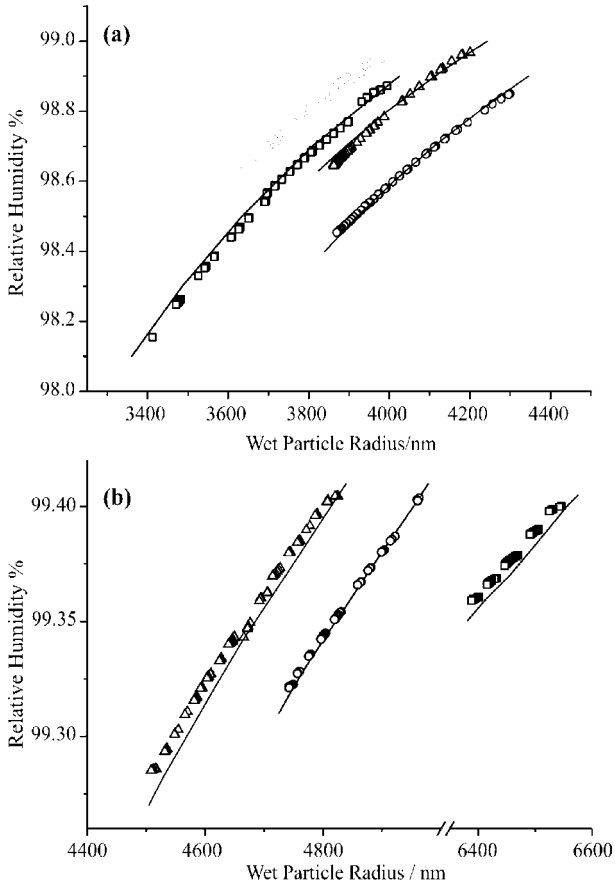

Figure 8. (a) Comparison of model predictions (ADDEM) and experimental measurements for four GA/SC droplets of GA/SC mass ratio 0.47, 2.11, 0.99 and 1.22 (left to right, respectively). (b) Comparison of model predictions (ADDEM) and experimental measurements for three GA/AS droplets of GA/AS mass ratio 5.02, 5.88 and 1.97 (left to right, respectively).

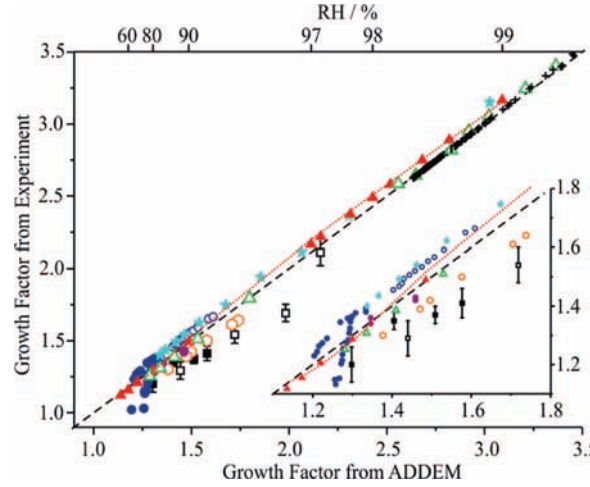

Figure 9. Comparison of experimentally measured and calculated growth factors with predictions from ADDEM. Open symbols correspond to the GA/SC system and filled symbols to the GA/AS system. Squares: Cruz and Pandis, ref 31; blue circles: Choi and Chan, ref 26; purple circles: Chan et al., ref 18; stars: bulk data from Choi and Chan, ref 26; hexagons: Prenni et al., ref 30; triangles: comparison of CSB-Fit with ADDEM; crosses: this data >98% RH for GA/SC system. A comparison of the GFP with ADDEM is shown by the dotted red line for the GA/AS system with a GA/AS mass ratio of 1.573, and the RH range is shown (top axis) for this system to provide a guide as to the RH range. The black dashed line is the 1:1 line. An insert shows the behavior at low growth factors/RHs in detail.

so that the water activity of the droplets at equilibrium is treated as equivalent to the RH in the system.

B. Aerosol Diameter Dependent Equilibrium Model (ADDEM). Calculations of the ZSR-based water activities of the solution droplets, including the Kelvin effect due to surface curvature, were carried out using the ADDEM model.[2,36] The RH, temperature and amounts of solute present are given as input, and an iterative procedure is used to determine the equilibrium droplet size. In this model, an external Newton−Raphson iterative loop is used to find a solution to the Köhler equation, and a constrained nonlinear minimization technique calculates the water activity for a given composition and set of conditions.

C. Dissociation of Glutaric Acid. Glutaric acid dissociates in aqueous solution, and has a first dissociation constant of 4.571×10^{-5} mol kg^{-1} at 298.15 K.[50] In the experiments described here dissociation is likely to be most significant in mixtures with AS, due to HSO_4^- formation. Dissociation was included in the E-AIM calculations, so that the ionic component of the solution contained either the ions Na^+, Cl^-, H^+, $HGlu^-$ (hydrogen glutarate), and Glu^{2-} (glutarate); or NH_4^+, SO_4^{2-},

HSO_4^-, H^+, $HGlu^-$, and Glu^{2-}. Parameters for the interactions between the cations and organic anions were assumed to be the same as those between each cation and HSO_4^- (for $HGlu^-$), and SO_4^{2-} (for Glu^{2-}). However, comparisons with calculations in which the dissociation of the acid was prevented showed that the effect on droplet water content was very small and could be neglected.

Acknowledgements. .

The authors acknowledge NERC for providing financial support for this work through the APPRAISE programme. K.L.H. acknowledges NERC for studentship support. J.P.R., L.M. and K.L.H. also acknowledge helpful discussions with Jason Butler during the course of this work.

References and Notes

(1) Clegg, S. L.; Brimblecombe, P.; Wexler, A. S. *J. Phys. Chem. A* **1998**, *102*, 2155–2171.

(2) Topping, D. O.; McFiggans, G. B.; Coe, H. *Atmos. Chem. Phys.* **2005**, *5*, 1205–1222.

(3) McFiggans, G.; Artaxo, P.; Baltensperger, U.; Coe, H.; Facchini, M. C.; Feingold, G.; Fuzzi, S.; Gysel, M.; Laaksonen, A.; Lohmann, U.; Mentel, T. F.; Murphy, D. M.; O'Dowd, C. D.; Snider, J. R.; Weingartner, E. *Atmos. Chem. Phys.* **2006**, *6*, 2593–2649.

(4) Climate Change 2007: The Physical Science Basis, Contribution of Working Group to the Fourth Assessment Report of the Intergovernmental Panel on Climate Change (IPCC) (2007).

(5) Marcolli, C.; Krieger, U. K. *J. Phys. Chem. A* **2006**, *110*, 1881–1893.

(6) Raatikainen, T.; Laaksonen, A. *Atmos. Chem. Phys.* **2005**, *5*, 2475–2495.

(7) Saxena, P.; Hildemann, L. M. *J. Atmos. Chem.* **1996**, *24*, 57–109.

(8) Svenningsson, B.; Rissler, J.; Swietlicki, E.; Mircea, M.; Bilde, M.; Facchini, M. C.; Decesari, S.; Fuzzi, S.; Zhou, J.; Monster, J.; Rosenorn, T. *Atmos. Chem. Phys.* **2006**, *6*, 1937–1952.

(9) Clegg, S. L.; Seinfeld, J. H. *J. Phys. Chem. A* **2006**, *110*, 5692–5717.

(10) Erdakos, G. B.; Asher, W. E.; Seinfeld, J. H.; Pankow, J. F. *Atmos. Environ.* **2006**, *40*, 6410–6421.

(11) Clegg, S. L.; Seinfeld, J. H.; Brimblecombe, P. *J. Aerosol Sci.* **2001**, *32*, 713–738.

(12) Clegg, S. L.; Seinfeld, J. H. *J. Phys. Chem. A* **2006**, *110*, 5718–5734.

(13) Rissman, T. A.; Varutbangkul, V.; Surratt, J. D.; Topping, D. O.; McFiggans, G.; Flagan, R. C.; Seinfeld, J. H. *Atmos. Chem. Phys.* **2007**, *7*, 2949–2971.

(14) Topping, D. O.; McFiggans, G. B.; Kiss, G.; Varga, Z.; Facchini, M. C.; Decesari, S.; Mircea, M. *Atmos. Chem. Phys.* **2007**, *7*, 2371–2398.

(15) Chan, M. N.; Lee, A. K. Y.; Chan, C. K. *Environ. Sci. Technol.* **2006**, *40*, 6983–6989.

(16) Chuang, P. Y. *J. Geophys. Res.−Atmos.* **2003**, *108*, 4282.

(17) Shulman, M. L.; Charlson, R. J.; Davis, E. J. *J. Aerosol Sci.* **1997**, *28*, 737–752.

(18) Chan, M. N.; Chan, C. K. *Atmos. Chem. Phys.* **2005**, *5*, 2703–2712.

(19) Butler, J. R.; Mitchem, L.; Hanford, K. L.; Treuel, L.; Reid, J. P. *Faraday Discuss.* **2008**, *137*, 351–366.

(20) Buajarern, J.; Mitchem, L.; Reid, J. P. *J. Phys. Chem. A* **2007**, *111*, 9054–9061.

(21) Buajarern, J.; Mitchem, L.; Reid, J. P. *J. Phys. Chem. A* **2007**, *111*, 11852–11859.

(22) Buajarern, J.; Mitchem, L.; Reid, J. P. *J. Phys. Chem. A* **2007**, *111*, 13038–13045.

(23) Riipinen, I.; Koponen, I. K.; Frank, G. P.; Hyvaerinen, A. P.; Vanhanen, J.; Lihavainen, H.; Lehtinen, K. E. J.; Bilde, M.; Kulmala, M. *J. Phys. Chem. A* **2007**, *111*, 12995–13002.

(24) Koehler, K. A.; Kreidenweis, S. M.; DeMott, P. J.; Prenni, A. J.; Carrico, C. M.; Ervens, B.; Feingold, G. *Atmos. Chem. Phys.* **2006**, *6*, 795–809.

(25) S. L. Clegg and A. S. Wexler, Extended Aerosol Inorganics Model (E-AIM), 2008 (http://www.aim.env.uea.ac.uk/aim/aim.php). This model incorporates the inorganic thermodynamic model described in ref 45, and adds a number of dicarboxylic acids (including glutaric acid). The water and solute activities of these acids are calculated using the treatment described in ref 9

(26) Choi, M. Y.; Chan, C. K. *Environ. Sci. Technol.* **2002**, *36*, 2422–2428.

(27) JordanovR., N.; Zellner, *Phys. Chem. Chem. Phys.* **2006**, *8*, 2759–2764.

(28) Pant, A.; Fok, A.; Parsons, M. T.; Mak, J.; Bertram, A. K. *Geophys. Res. Lett.* **2004**, *31*.

(29) Parsons, M. T.; Knopf, D. A.; Bertram, A. K. *J. Phys. Chem. A* **2004**, *108*, 11600–11608.

(30) Prenni, A. J.; De Mott, P. J.; Kreidenweis, S. M. *Atmos. Environ.* **2003**, *37*, 4243–4251.

(31) Cruz, C. N.; Pandis, S. N. *Environ. Sci. Technol.* **2000**, *34*, 4313–4319.

(32) Mitchem, L.; Buajarern, J.; Hopkins, R. J.; Ward, A. D.; Gilham, R. J. J.; Johnston, R. L.; Reid, J. P. *J. Phys. Chem. A* **2006**, *110*, 8116–8125.

(33) Knox, K. J.; Reid, J. P.; Hanford, K. L.; Hudson, A. J.; Mitchem, L. *J. Optics A: Pure Appl. Optics* **2007**, *9*, S180–S188.

(34) Mitchem, L.; Reid, J. P. *Chem. Soc. Rev.* **2008**, *37*, 756–769.

(35) Reid, J. P.; Meresman, H.; Mitchem, L.; Symes, R. *Int. Rev. Phys. Chem.* **2007**, *26*, 139–192.

(36) Topping, D. O.; McFiggans, G. B.; Coe, H. *Atmos. Chem. Phys.* **2005**, *5*, 1223–1242.

(37) Kreidenweis, S. M.; Koehler, K.; DeMott, P. J.; Prenni, A. J.; Carrico, C.; Ervens, B. *Atmos. Chem. Phys.* **2005**, *5*, 1357–1370.

(38) Archer, D. G. *J. Phys. Chem. Ref. Data* **1992**, *21*, 793–829.

(39) Clegg, S. L.; Ho, S. S.; Chan, C. K.; Brimblecombe, P. *J. Chem. Eng. Data* **1995**, *40*, 1079–1090.

(40) Fredenslund, A.; Jones, R. L.; Prausnitz, J. M. *AIChE J.* **1975**, *21*, 1086–1098.

(41) Peng, C.; Chan, M. N.; Chan, C. K. *Environ. Sci. Technol.* **2001**, *35*, 4495–4501.

(42) Stokes, R. H.; Robinson, R. A. *J. Phys. Chem.* **1966**, *70*, 2126–2130.

(43) Clegg, S. L.; Seinfeld, J. H. *J. Phys. Chem. A* **2004**, *108*, 1008.

(44) K. S. Pitzer, In: *Activity Coefficients in Electrolyte Solutions*, 2nd ed.; K. S. Pitzer Ed.; CRC Press: Boca Raton, FL, 1991; pp 75−154.

(45) Wexler, A. S.; Clegg, S. L. *J. Geophys. Res. 107*, (D14), 4207, doi: 10.1029/2001JD000451.

(46) Tang, I. N. *J. Geophys. Res.* **1997**, *102* (D2), 1883–1893.

(47) Gaman, A. I.; Kulmala, M.; Vehkamaki, H.; Napari, I.; Mircea, M.; Facchini, M. C.; Laaksonen, A. *J. Chem. Phys.* **2004**, *120*, 282–291.

(48) Li, Z. B.; Lu, B. C. Y. *Chem. Eng. Sci.* **2001**, *56*, 2879–2888.

(49) Chen, J. P. *J. Atmos. Sci.* **1994**, *51*, 3505–3516.

(50) Jones, R. H.; Stock, D. I. *J. Chem. Soc.* **1960**, 102–105.

JP802520D